

Triadic approximation for contagions on higher-order networks

Giulio Burgio, Sergio Gómez, and Alex Arenas
*Departament d'Enginyeria Informàtica i Matemàtiques,
Universitat Rovira i Virgili, 43007 Tarragona, Spain*

Based on mechanisms of social reinforcement, complex contagion processes where transmission depends on the simultaneous exposure to multiple sources are a peculiar feature of human social systems. Such processes rely on many-body interactions and hypergraphs provide a suitable representation for them. Considering up to three-body interactions, we derive a mean-field model going beyond limiting node- and pair-based approximations. We reveal in this way how the stability of the contagion-free state is affected by both the two- and the three-body infection rates, and relate it to the degree of overlap between three- and two-body interactions. We show the double-edged effect of an increased overlap, yielding a lower critical point but at the expense of a smaller outbreak. Our results, corroborated by numerical simulations on hypergraphs which are either synthetic or constructed from real-world proximity data, underline the importance of the chosen representation to describe a higher-order process.

Behaviors, strategies, norms, conventions and other social entities often require some form of reinforcement for their adoption [1, 2]. Spreading among individuals through learning and imitation, their diffusion can be studied as a contagion process. Differently from epidemics, however, repeated exposures to the same contagious source (e.g., an individual with a given behavior) are not always sufficient for transmission and multiple sources are required, defining a complex contagion [1]. When transmission depends on the multiple exposures being simultaneous, a spreading event needs to be described as a many-body interaction, not reducible to a sum of two-body interactions [3].

The social contagion can be mapped to a susceptible-infectious-susceptible (SIS) process on a hypergraph [3–5], where an n -body interaction is represented by an n -edge (i.e., an edge of cardinality n) [6]. We assume that a susceptible individual becomes infected at rate $\beta^{(1)}$ during a two-body interaction (a 2-edge) with an infected individual ($S + I \rightarrow 2I$), at rate $\beta^{(2)}$ during a three-body interaction (a 3-edge) with two infected individuals ($S + 2I \rightarrow 3I$), and so on for larger groups. Infected individuals recover at rate μ ($I \rightarrow S$). In this setting, previous models using node-based (uncorrelated states) approximations found that the critical pairwise threshold, $\beta_{\text{cr}}^{(1)}$, at which the free (fully susceptible) state becomes unstable, is independent from the higher-order couplings $\{\beta^{(n)}\}_{n>1}$, no matter the properties of the interaction hypergraph [3, 4]. This is however in clear disagreement with numerical simulations [3, 5]. In fact, by means of a microscopic model taking into account the dynamical correlations emerging within groups, we predicted how $\beta^{(2)}$ affects $\beta_{\text{cr}}^{(1)}$ in several quenched structures [5]. This is found by solving an implicit equation involving the spectral radius of a certain matrix. The complicated form this matrix generally takes, however, prevents to find an explicit formula for $\beta_{\text{cr}}^{(1)}$, leaving the functional form of the latter unknown and thus unclear how it is affected by the properties of the interaction structure.

In this work, we fill this gap by deriving a mean-field

model that reveals how the stability of the free state depends either on the couplings $\beta^{(1)}$ and $\beta^{(2)}$, and on the degree of overlap between three- and two-body interactions. We derive a closed-form formula for the critical surface and prove that $\beta_{\text{cr}}^{(1)}$ can be made arbitrarily small by increasing $\beta^{(2)}$. Such dependence is maximal in a simplicial complex, where $\beta_{\text{cr}}^{(1)}$ is minimized, and disappears instead in a linear hypergraph, the three-body interactions being not supported by the two-body ones in this case. Nevertheless, linear hypergraphs ensure the largest contagions for strong enough couplings. Numerical simulations on either synthetic hypergraphs and hypergraphs constructed from real-world proximity data corroborate our predictions.

We start from a set of exact microscopic equations on which to apply a closure approximation. We keep track of the state evolution of subsets of nodes which form cliques in the projection graph (i.e., the graph constructed by associating cliques to edges of the hypergraph). The closure we use exclusively relies on maximal cliques (i.e., not subset of larger ones). Accordingly, considering up to three-body interactions (i.e., rank-3 hypergraphs), we account for the evolution of the state probability $P_i^{\sigma_i}$ for node i to be in state σ_i , $P_{ij}^{\sigma_i\sigma_j}$ for the maximal link ij to be in state $\sigma_i\sigma_j$, $P_{ijl}^{\sigma_i\sigma_j\sigma_l}$ for the (maximal) 3-clique ijl to be in state $\sigma_i\sigma_j\sigma_l$. Notice that a 3-clique, when projected back to the hypergraph, comes in one of three flavors: a length-3 cycle (or 3-cycle), conveying only two-body interactions, a 3-edge, conveying only a three-body interaction, or a 2-simplex (or triangle), conveying all of them.

The state probability of any other local structure is approximated in terms of the maximal cliques composing it. We consider random hypergraphs that are sparse to the extent that the probability for two maximal cliques to share more than one node vanishes in the thermodynamic limit. This requires the number of maximal edges of any cardinality to scale slower than quadratically with the system size. We thus need a closure only for the following local structures: two connected maximal links, a

maximal link connected to a 3-clique, and two connected 3-cliques. We approximate their state as follows [5]

$$P_{ijl}^{\sigma_i \sigma_j \sigma_l} \approx P_{ij}^{\sigma_i \sigma_j} P_{jl}^{\sigma_j \sigma_l} / P_j^{\sigma_j} \quad (1a)$$

$$P_{ijlh}^{\sigma_i \sigma_j \sigma_l \sigma_h} \approx P_{ij}^{\sigma_i \sigma_j} P_{jlh}^{\sigma_j \sigma_l \sigma_h} / P_j^{\sigma_j} \quad (1b)$$

$$P_{ijlhk}^{\sigma_i \sigma_j \sigma_l \sigma_h \sigma_k} \approx P_{ijl}^{\sigma_i \sigma_j \sigma_l} P_{lhk}^{\sigma_l \sigma_h \sigma_k} / P_l^{\sigma_l} \quad (1c)$$

where the underline indicates the central, bridging node. We refer to Eqs. (1) as the *triadic approximation*.

The higher-order interaction structure is encoded in the following binary tensors: $A^{(1)}$, such that $A_{ij}^{(1)} = 1$ if the maximal link ij exists; $A^{(1,0)}$ and $A^{(0,1)}$, such that $A_{ijl}^{(1,0)} = 1$ ($A_{ijl}^{(0,1)} = 0$) and $A_{ijl}^{(0,1)} = 0$ ($A_{ijl}^{(1,0)} = 1$) if

ijl is a 3-cycle (3-edge); and such that $A_{ijl}^{(1,0)} A_{ijl}^{(0,1)} = 1$ if ijl is a triangle (for later convenience, we introduce $A^{(1,1)} = A^{(1,0)} \odot A^{(0,1)}$). Specifically, if for any 3-clique ijl , $A_{ijl}^{(0,1)} = 1 \Rightarrow A_{ijl}^{(1,0)} = 1$, the hypergraph is a simplicial 2-complex [7]. If, instead, $A_{ijl}^{(0,1)} = 1 \Rightarrow A_{ijl}^{(1,0)} = 0$, it is a linear hypergraph [8] (any of the non-maximal links ij , il and jl , is excluded by the assumed sparsity). Any hypergraph is located in between these two limits, depending on the degree of overlap between three- and two-body interactions.

The description of the process eventually consists of the following system of microscopic equations (notice time has been rescaled by μ)

$$\dot{P}_i^I = -P_i^I + \beta^{(1)} \sum_j A_{ij}^{(1)} P_{ij}^{SI} + \frac{1}{2} \sum_{j,l} \left[A_{ijl}^{(1,0)} \beta^{(1)} (P_{ijl}^{SSI} + P_{ijl}^{SIS} + 2P_{ijl}^{SII}) + A_{ijl}^{(0,1)} \beta^{(2)} P_{ijl}^{SII} \right] \quad (2a)$$

$$\begin{aligned} \dot{P}_{ij}^{SI} = & -(1 + \beta^{(1)}) P_{ij}^{SI} + P_{ij}^{II} - \beta^{(1)} \sum_{l \neq j} A_{il}^{(1)} P_{jil}^{SI} + \beta^{(1)} \sum_{l \neq i} A_{jl}^{(1)} P_{ijl}^{SSI} \\ & - \frac{1}{2} \sum_{l,h} \left[A_{ilh}^{(1,0)} \beta^{(1)} (P_{jilh}^{ISIS} + P_{jilh}^{ISSI} + 2P_{jilh}^{ISII}) + A_{ilh}^{(0,1)} \beta^{(2)} P_{jilh}^{ISII} \right] + \{i \leftrightarrow j\} \end{aligned} \quad (2b)$$

$$\begin{aligned} \dot{P}_{ijl}^{SSI} = & -(1 + 2A_{ijl}^{(1,0)} \beta^{(1)}) P_{ijl}^{SSI} + P_{ijl}^{ISI} + P_{ijl}^{SII} \\ & - \beta^{(1)} \sum_{h \neq j,l} A_{ih}^{(1)} P_{jlih}^{SISI} - \beta^{(1)} \sum_{h \neq i,l} A_{jh}^{(1)} P_{iljh}^{SISI} + \beta^{(1)} \sum_{h \neq i,j} A_{lh}^{(1)} P_{ijlh}^{SSSI} \\ & - \frac{1}{2} \sum_{h,k \neq j,l} \left[A_{ihk}^{(1,0)} \beta^{(1)} (P_{jlih}^{SISIS} + P_{jlih}^{SISSI} + 2P_{jlih}^{SISII}) + A_{ihk}^{(0,1)} \beta^{(2)} P_{jlih}^{SISII} \right] - \{i \leftrightarrow j\} + \{i \leftrightarrow l\} \end{aligned} \quad (2c)$$

$$\begin{aligned} \dot{P}_{ijl}^{SII} = & -(2 + 2A_{ijl}^{(1,0)} \beta^{(1)} + A_{ijl}^{(0,1)} \beta^{(2)}) P_{ijl}^{SII} + A_{ijl}^{(1,0)} \beta^{(1)} (P_{ijl}^{SSI} + P_{ijl}^{SIS}) + P_{ijl}^{III} \\ & - \beta^{(1)} \sum_{h \neq j,l} A_{ih}^{(1)} P_{jlih}^{IISI} + \beta^{(1)} \sum_{h \neq i,l} A_{jh}^{(1)} P_{iljh}^{IISI} + \beta^{(1)} \sum_{h \neq i,j} A_{lh}^{(1)} P_{ijlh}^{SISI} \\ & - \frac{1}{2} \sum_{h,k \neq j,l} \left[A_{ihk}^{(1,0)} \beta^{(1)} (P_{jlih}^{IISIS} + P_{jlih}^{IISSI} + 2P_{jlih}^{IISII}) + A_{ihk}^{(0,1)} \beta^{(2)} P_{jlih}^{IISII} \right] + \{i \leftrightarrow j\} + \{i \leftrightarrow l\} \end{aligned} \quad (2d)$$

where $\{i \leftrightarrow j\}$ is a short notation to denote the term obtained by swapping i and j in the explicit term (excluding the sign in front) on the same line. The other state probabilities are found as $P_i^S = 1 - P_i^I$, $P_{ij}^{SS} = 1 - P_i^I - P_{ij}^{SI}$, $P_{ij}^{II} = P_i^I - P_{ij}^{IS}$, $P_{ijl}^{SSS} = 1 - P_i^I - P_{ijl}^{SII} - P_{ijl}^{SSI} - P_{ijl}^{SIS}$, $P_{ijl}^{III} = P_i^I - P_{ijl}^{IISI} - P_{ijl}^{IIS} - P_{ijl}^{IIS}$ [9]. Eqs. (2) are closed through Eqs. (1). The system consists then of $N + L + 2(T^{(1,0)} + T^{(0,1)} + T^{(1,1)})$ equations, being N , L , $T^{(1,0)}$, $T^{(0,1)}$ and $T^{(1,1)}$, the number of nodes, maximal links, 3-cycles, 3-edges and triangles, respectively.

To make this model analytically treatable, we perform a mean-field dimensional reduction by regarding all the nodes and cliques as equivalent to their average counterparts. Accordingly, every node is assumed to be part of the same number of maximal links, $k^{(1)}$, 3-cliques, $k^{(1,0)}$, 3-edges, $k^{(0,1)}$, and triangles, $k^{(1,1)}$;

and thus participates in $\kappa^{(1)} = k^{(1)} + 2(k^{(1,0)} + k^{(1,1)})$ two-body interactions and $\kappa^{(2)} = k^{(1,0)} + k^{(1,1)}$ three-body interactions (see Fig. 1 for illustration). The state probabilities P_i^σ , $P_{ij}^{\sigma\sigma'}$ and $P_{ijl}^{\sigma\sigma'\sigma''}$, with $\sigma, \sigma', \sigma'' \in \{S, I\}$, are taken equal to their respective averages, $P^\sigma = \sum_i P_i^\sigma / N$, $P^{\sigma\sigma'} = \sum_{i,j} A_{ij}^{(1)} P_{ij}^{\sigma\sigma'} / Nk^{(1)}$ and $P_x^{\sigma\sigma'\sigma''} = \sum_{i,j,l} A_{ijl}^x P_{ijl}^{\sigma\sigma'\sigma''} / 2Nk^x$, where the index $x \in \{(1,0), (0,1), (1,1)\}$ denotes the type of the considered 3-clique. Since we are considering undirected structures, note that permuting the upper, state indices has no effect.

Introduced the indicator function $\mathbb{1}_p$, giving 1 if condition p is fulfilled and 0 otherwise, the reduced system reads

$$\dot{P}^I = -P^I + \beta^{(1)}k^{(1)}P^{SI} + 2\beta^{(1)}\left[k^{(1,0)}(P_{(1,0)}^{SSI} + P_{(1,0)}^{SII}) + k^{(1,1)}(P_{(1,1)}^{SSI} + P_{(1,1)}^{SII})\right] + \beta^{(2)}\left[k^{(0,1)}P_{(0,1)}^{SII} + k^{(1,1)}P_{(1,1)}^{SII}\right] \quad (3a)$$

$$\begin{aligned} \dot{P}^{SI} = & -(1 + \beta^{(1)})P^{SI} + P^{II} - \beta^{(1)}(k^{(1)} - 1)P^{SI}\frac{P^{SI} - P^{SS}}{PS} \\ & - \left\{2\beta^{(1)}\left[k^{(1,0)}(P_{(1,0)}^{SSI} + P_{(1,0)}^{SII}) + k^{(1,1)}(P_{(1,1)}^{SSI} + P_{(1,1)}^{SII})\right] + \beta^{(2)}\left[k^{(0,1)}P_{(0,1)}^{SII} + k^{(1,1)}P_{(1,1)}^{SII}\right]\right\}\frac{P^{SI} - P^{SS}}{PS} \end{aligned} \quad (3b)$$

$$\begin{aligned} \dot{P}_x^{SSI} = & -2(1 + \beta^{(1)}\mathbb{1}_{x \neq (0,1)})P_x^{SSI} + 2P_x^{SII} - \beta^{(1)}k^{(1)}P^{SI}\frac{2P_x^{SSI} - P_x^{SSS}}{PS} \\ & - 2\beta^{(1)}\left[(k^{(1,0)} - \mathbb{1}_{x=(1,0)})(P_{(1,0)}^{SSI} + P_{(1,0)}^{SII}) + (k^{(1,1)} - \mathbb{1}_{x=(1,1)})(P_{(1,1)}^{SSI} + P_{(1,1)}^{SII})\right]\frac{2P_x^{SSI} - P_x^{SSS}}{PS} \\ & - \beta^{(2)}\left[(k^{(0,1)} - \mathbb{1}_{x=(0,1)})P_{(0,1)}^{SII} + (k^{(1,1)} - \mathbb{1}_{x=(1,1)})P_{(1,1)}^{SII}\right]\frac{2P_x^{SSI} - P_x^{SSS}}{PS} \end{aligned} \quad (3c)$$

$$\begin{aligned} \dot{P}_x^{SII} = & -(2 + 2\beta^{(1)}\mathbb{1}_{x \neq (0,1)} + \beta^{(2)}\mathbb{1}_{x \neq (1,0)})P_x^{SII} + 2\beta^{(1)}\mathbb{1}_{x \neq (0,1)}P_x^{SSI} + P_x^{III} - \beta^{(1)}k^{(1)}P^{SI}\frac{P_x^{SII} - 2P_x^{SSI}}{PS} \\ & - 2\beta^{(1)}\left[(k^{(1,0)} - \mathbb{1}_{x=(1,0)})(P_{(1,0)}^{SSI} + P_{(1,0)}^{SII}) + (k^{(1,1)} - \mathbb{1}_{x=(1,1)})(P_{(1,1)}^{SSI} + P_{(1,1)}^{SII})\right]\frac{P_x^{SII} - 2P_x^{SSI}}{PS} \\ & - \beta^{(2)}\left[(k^{(0,1)} - \mathbb{1}_{x=(0,1)})P_{(0,1)}^{SII} + (k^{(1,1)} - \mathbb{1}_{x=(1,1)})P_{(1,1)}^{SII}\right]\frac{P_x^{SII} - 2P_x^{SSI}}{PS} \end{aligned} \quad (3d)$$

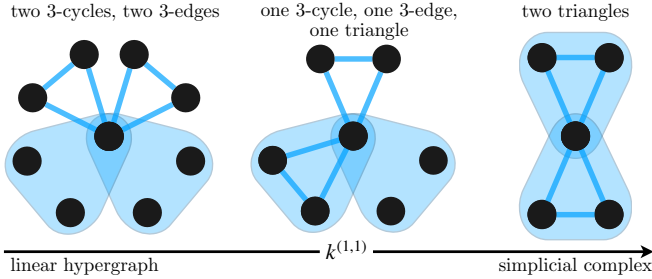


FIG. 1. Example showing how the neighbourhood of a focal node changes with $k^{(1,1)}$ for fixed degrees $\kappa^{(1)}$, $k^{(1)}$ (zero here) and $\kappa^{(2)}$. The node takes always part to $\kappa^{(1)} = 4$ two-body interactions and $\kappa^{(2)} = 2$ three-body interactions, but their degree of overlap changes.

where $P^S = 1 - P^I$, $P^{SS} = 1 - P^I - P^{SI}$, $P^{II} = P^I - P^{SI}$, $P^{SSS} = 1 - P^I - P^{SII} - 2P^{SSI}$, $P^{III} = P^I - P^{SSI} - 2P^{SII}$.

In order to correctly locate the phase transition, we linearize Eqs. (3) around the free state by regarding of the same order $\epsilon \ll 1$ the probabilities of infected states, i.e., $P^I, P^{SI}, P^{II}, P_x^{SSI}, P_x^{SII}, P_x^{III} \sim \mathcal{O}(\epsilon)$ [5]. The right-most eigenvalue of the Jacobian matrix associated to the resulting linear system crosses the imaginary axis when the following condition is satisfied,

$$k^{(1)}\frac{\beta^{(1)}}{1 + \beta^{(1)}} + k^{(1,0)}\frac{2\beta^{(1)}(1 + \beta^{(1)})}{1 + 2\beta^{(1)}(1 + \beta^{(1)})} + k^{(1,1)}\frac{\beta^{(1)}(2 + 2\beta^{(1)} + \beta^{(2)})}{1 + \beta^{(1)}(2 + 2\beta^{(1)} + \beta^{(2)})} = 1 \quad (4)$$

Eq. (4) defines the critical surface in the parameter space. We first observe that it has no solution when either $\beta^{(1)} = 0$ or there are only three-body interactions ($\kappa^{(2)} = k^{(0,1)}$ and $\kappa^{(1)} = 0$), for $k^{(0,1)}$ does not appear. This reveals that a three-body interaction cannot affect the stability of the free state unless “activated” by the presence of two-body interactions within the same subset of nodes. Two-body interactions are thus needed to destabilize the free state. That activation occurs in triangles. Indeed, if $k^{(1,1)} > 0$, since each term in the l.h.s. of Eq. (4) is

a strictly increasing function of the infection rates, the larger is $\beta^{(1)}$ ($\beta^{(2)}$), the smaller is $\beta^{(2)} = \beta_{\text{cr}}^{(2)}$ ($\beta^{(1)} = \beta_{\text{cr}}^{(1)}$) solving Eq. (4). $\beta_{\text{cr}}^{(2)}$ is a monotonically decreasing function of $\beta^{(1)}$, diverging positively as $1/\beta^{(1)}$ for $\beta^{(1)} \rightarrow 0$. Put differently, $\beta_{\text{cr}}^{(1)}$ can be made arbitrarily small by increasing $\beta^{(2)}$. Moreover, imposing $\beta^{(2)} = 0$, one finds that $\beta_{\text{cr}}^{(2)}$ crosses zero (where pairwise interactions alone suffice to cause extensive spreads) at a finite $\beta^{(1)}$ in the interval $[\beta_{(1)}^{(1)}, \beta_{(1,0)}^{(1)}]$, being $\beta_{(1)}^{(1)} = 1/(\kappa^{(1)} - 1)$ and

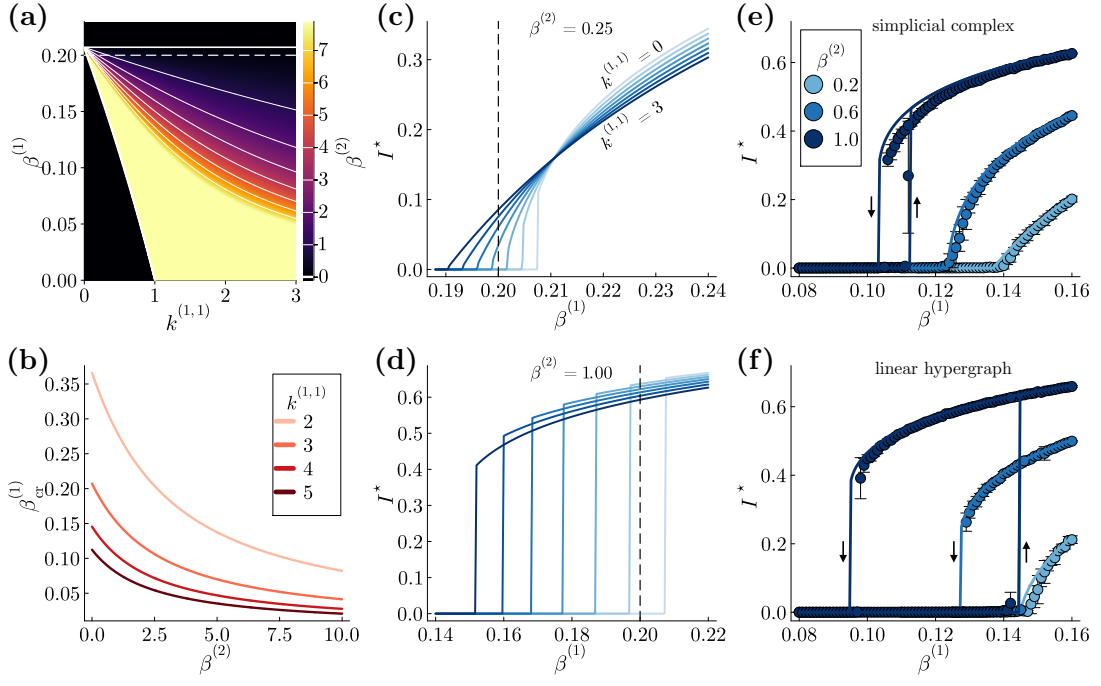


FIG. 2. Predictions from the mean-field model. (a) Critical surface $(k^{(1,1)}, \beta^{(1)}, \beta^{(2)})$ defined by Eq. (4) for hypergraphs with $\kappa^{(1)} = 6$ two-body interactions ($k^{(1)} = 0$) and $\kappa^{(2)} = 3$ three-body interactions per node. The white solid curves correspond to the values of $\beta^{(2)}$ indicated in the colorbar (limited at 7 for better readability), the curve $\beta^{(2)} = 0$ being thicker. The horizontal dashed line indicates $\beta^{(1)} = 1/5$, the threshold for the locally tree-like network with same $\kappa^{(1)}$. (b) Critical threshold $\beta_{\text{cr}}^{(1)} \equiv \beta_{(1,1)}^{(1)}$, Eq. (5), for homogeneous simplicial 2-complex of various connectivity. (c)–(d) Equilibrium fraction of infected nodes (fixed point of Eqs. (3)), I^* , for $\beta^{(2)} = 0.25, 1.00$ and $k^{(1,1)}$ from 0 (lightest shade) to 3 (darkest shade) in steps of 0.5. The vertical dashed line indicates $\beta_{(1)}^{(1)} = 1/5$. (e)–(f) Comparison with the results from numerical simulations performed on random regular hypergraphs with $N = 5000$, $\kappa^{(1)} = 8$, $k^{(1)} = 2$, $\kappa^{(2)} = 3$, and $k^{(1,1)} = 3$ (simplicial complex) and $k^{(1,1)} = 0$ (linear hypergraph). Points and error bars denote averages and standard errors computed over 20 random initializations. Upward and downward arrows indicate the forward and backward curves whenever a hysteresis cycle exists.

$\beta_{(1,0)}^{(1)} = (\sqrt{1 + 4/(\kappa^{(1)} - 2)} - 1)/2$ the critical point for, respectively, a locally tree-like network ($\kappa^{(2)} = 0$ and $\kappa^{(1)} = k^{(1)}$) and a 3-cycle-based network ($\kappa^{(2)} = 0$ and $\kappa^{(1)} = 2k^{(1,0)}$). It is easy to see that $\beta_{(1,0)}^{(1)} > \beta_{(1)}^{(1)}$, in accordance with previous studies proving that the critical point is raised by clustering [10, 11].

Considering then a triangle-based network ($\kappa^{(2)} = k^{(1,1)}$ and $\kappa^{(1)} = 2k^{(1,1)}$), i.e., a homogeneous simplicial 2-complex, we find that the critical point, $\beta_{(1,1)}^{(1)}$, reads

$$\beta_{(1,1)}^{(1)} = \frac{\beta^{(2)} + 2}{4} \left[\sqrt{1 + \frac{16}{(\kappa^{(1)} - 2)(\beta^{(2)} + 2)^2}} - 1 \right] \quad (5)$$

$\beta_{(1,1)}^{(1)}$ diverges for $\kappa^{(1)} \rightarrow 2^+$ ($k^{(1,1)} \rightarrow 1^+$), consistently with the fact that an extensive contagion can occur only if a giant component exists, and vanishes for $\beta^{(2)} \rightarrow \infty$ (see Fig. 2(b)), as already stated for the general case. Observe that, for large $\kappa^{(1)}$, like $\partial\beta_{(1)}^{(1)}/\partial\kappa^{(1)}$, also $\partial\beta_{(1,1)}^{(1)}/\partial\kappa^{(1)} \sim 1/\kappa^{(1)^2}$. Lastly, notice that the threshold for the 3-cycle-based network, $\beta_{(1,0)}^{(1)}$, is recovered taking $\beta^{(2)} = 0$.

To isolate the effect of the overlap between two- and three-body interactions, we fix $\kappa^{(1)}$, $k^{(1)}$ and $\kappa^{(2)}$, and increase $k^{(1,1)}$ from 0 to $\min\{(\kappa^{(1)} - k^{(1)})/2, \kappa^{(2)}\}$ (correspondingly, $k^{(1,0)} = (\kappa^{(1)} - k^{(1)})/2 - k^{(1,1)}$ and $k^{(0,1)} = \kappa^{(2)} - k^{(1,1)}$ decrease). Importantly, as illustrated in Fig. 1, a larger $k^{(1,1)}$ implies a smaller and more redundant neighbourhood. One may thus expect that the critical point increases with $k^{(1,1)}$. As detailedly shown in Fig. 2, instead, either $\beta_{\text{cr}}^{(1)}$ and $\beta_{\text{cr}}^{(2)}$ decrease with $k^{(1,1)}$, taking the lowest values in a simplicial complex and the highest in a linear hypergraph. As we have learned, 3-edges yield a negligible contribution to the contagion at the early stage, therefore reducing them in favor of triangles helps the spread to become extensive. This holds also for the equilibrium fraction of infected nodes, I^* , when $\beta^{(2)}$ is small enough and $\beta^{(1)}$ is in a narrow range around the threshold $\beta_{(1)}^{(1)}$ for the corresponding locally tree-like network with same $\kappa^{(1)}$ (see Fig. 2(c)). For larger infection rates, that redundancy becomes eventually disadvantageous, for potentially infectious edges lead to nodes already infected and are therefore “wasted” (analogously to the effect of clustering). The largest

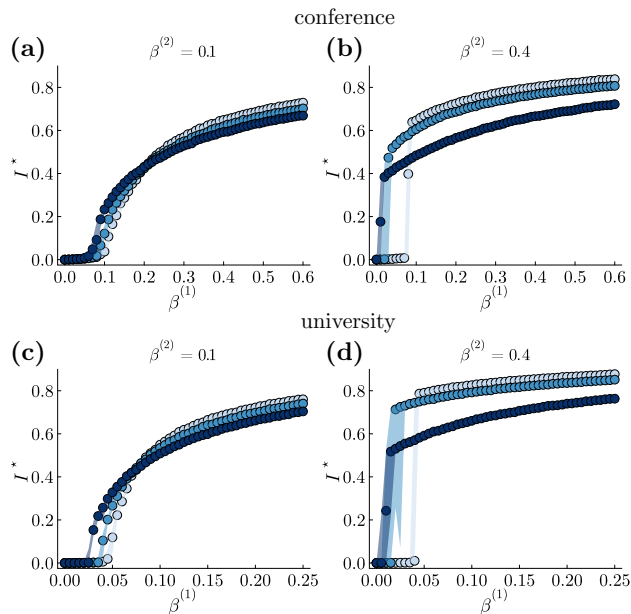


FIG. 3. Results from numerical simulations performed on rank-3 hypergraphs constructed from face-to-face interactions recorded during a conference [12] ((a)-(b)) and from proximity data recorded in a university campus [13] ((c)-(d)). Each point denotes the median computed over 20 random initializations, while the ribbon covers the interval from the 5-th to the 95-th percentile. From the lightest (linear hypergraph) to the darkest (simplicial complex) shade, the 0%, 50% and 100% of the added three-body interactions form triangles.

spreads are in such case found for $k^{(1,1)} = 0$ (i.e., linear hypergraphs), ensuring the least-redundant, widest neighbourhoods (see Fig. 2(d)).

We test the model on random regular hypergraphs. These are generated through a standard configuration model in which every node has assigned the same degrees $k^{(1)}$, $k^{(0,1)}$, $k^{(1,0)}$ and $k^{(1,1)}$. As reported in Figs. 2(e) and (f), the numerical simulations confirm the predictions made by the mean-field model.

We further test those predictions on hypergraphs we constructed from real-world data. One dataset contains face-to-face interactions recorded during a conference [12], the other one proximity data recorded within a university campus [13]. These are both time-resolved data which, once aggregated, yields very dense networks [12]. Aggregated each dataset into a static network where each link is assigned a weight equal to the number of times that link appears, we retain a portion of the links with highest weight (highest 5% for the con-

ference network and highest 25% for the university's) for which the network is still connected. The networks are then converted into binary ones and all their 3-cycles are computed. The resulting networks have, respectively, 219 and 672 nodes, and around 1200 and 15000 3-cycles. The hypergraphs are then constructed by adding a given number (respectively, around 650 and 3000) of three-body interactions to either 3-cycles, converting them in triangles, or to randomly selected triplets of unconnected nodes, forming 3-edges. As shown in Fig. 3, the simulations corroborate the uncovered phenomenology.

Through the derivation of a mean-field model, this study elucidates the dynamics of complex contagion processes within higher-order networks. The analysis extends beyond traditional node- and pair-based approximations, uncovering that three-body interactions contribute to destabilizing the free state, albeit their activation is contingent on overlapping with two-body interactions. Examining the boundary structures, it was established that simplicial complexes and linear hypergraphs — representing maximal and no overlap respectively — exert diametrically opposed dynamical effects. The simplicial complexes reduce the critical point, while often resulting in smaller contagion spread; conversely, linear hypergraphs heighten the critical point, typically leading to larger spread. Complementing recent findings on structure-dependent effects in synchronization [14], the current investigation underscores the necessity of identifying the most suitable representation for specific higher-order processes.

Acknowledgments. G.B. acknowledges financial support from the European Union's Horizon 2020 research and innovation program under the Marie Skłodowska-Curie Grant Agreement No. 945413 and from the Universitat Rovira i Virgili (URV). A.A. and S.G. acknowledge support by Ministerio de Economía y Competitividad (PID2021-128005NB-C21; RED2022-134890-T), Generalitat de Catalunya (2021SGR-633) and Universitat Rovira i Virgili (2022PFR-URV-56). AA also acknowledges the Joint Appointment Program at Pacific Northwest National Laboratory (PNNL). PNNL is a multi-program national laboratory operated for the U.S. Department of Energy (DOE) by Battelle Memorial Institute under Contract No. DE-AC05-76RL01830, the European Union's Horizon Europe Programme under the CREXDATA project, grant agreement no. 101092749, the ICREA Academia award, and the James S. McDonnell Foundation (Grant No. 220020325).

[1] D. Centola and M. Macy, American journal of Sociology **113**, 702 (2007).
 [2] D. Guilbeault, J. Becker, and D. Centola, Complex spreading phenomena in social systems: Influence and contagion in real-world social networks, 3 (2018).

[3] I. Iacopini, G. Petri, A. Barrat, and V. Latora, Nature communications **10**, 2485 (2019).
 [4] N. W. Landry and J. G. Restrepo, Chaos: An Interdisciplinary Journal of Nonlinear Science **30**, 103117 (2020).
 [5] G. Burgio, A. Arenas, S. Gómez, and J. T. Matamalas,

- Communications Physics **4**, 111 (2021).
- [6] F. Battiston, G. Cencetti, I. Iacopini, V. Latora, M. Lucas, A. Patania, J.-G. Young, and G. Petri, *Physics Reports* **874**, 1 (2020).
- [7] Strictly speaking, a simplicial complex requires the edge set to contain also the empty set and the singletons, i.e., the edges containing single nodes [8]. While the former has no physical meaning, the latter can be thought as representing the internal recovery dynamics of a node.
- [8] A. Bretto, *An introduction. Mathematical Engineering*. Cham: Springer (2013).
- [9] Notice that the meaning of any of such probabilities doesn't change when the same permutation is applied to both the upper and lower indices (e.g., $P_{ijl}^{ISl} \equiv P_{jil}^{SIl}$).
- [10] J. C. Miller, *Physical Review E* **80**, 020901 (2009).
- [11] L. Hébert-Dufresne, P.-A. Noël, V. Marceau, A. Allard, and L. J. Dubé, *Physical Review E* **82**, 036115 (2010).
- [12] M. Génois and A. Barrat, *EPJ Data Science* **7**, 1 (2018).
- [13] P. Sapiezynski, A. Stopczynski, D. D. Lassen, and S. Lehmann, *Scientific Data* **6**, 315 (2019).
- [14] Y. Zhang, M. Lucas, and F. Battiston, *Nature Communications* **14**, 1605 (2023).